Int. J. Multiphase Flow Vol. 15, No. 2, pp. 173–191, 1989
Printed in Great Britain.

0301-9322/89 $3.00 + 0.00

MODELING FLOW PATTERN TRANSITIONS FOR UPWARD GAS–LIQUID FLOW IN VERTICAL CONCENTRIC AND ECCENTRIC ANNULI

V. C. KELESSIDIS† and A. E. DUKLER‡
Department of Chemical Engineering, University of Houston, Houston, TX 77004, U.S.A.

(*Received* 24 *November* 1987; *in revised form* 1 *November* 1988)

Abstract—Flow patterns were investigated in vertical upward gas–liquid flow in a concentric and an eccentric annulus (eccentricity 50%). A new method for flow pattern identification is proposed based on probability density function analysis of conductance probe signals. Flow pattern maps have been constructed and mathematical models are proposed which predict the flow pattern transitions.

Key Words: gas–liquid flow, annulus, flow patterns

INTRODUCTION

Two-phase flow in concentric and eccentric annuli occurs in a variety of important practical situations. The influx of the gas into the wellbore of an oil well creates two-phase flow in an annulus. During measurements in oil wells, the presence of the instrument creates annular passages. Better understanding of two-phase flow in an annulus will provide more reliable design methods for many types of industrial equipment, e.g. double pipe heat exchangers, water-cooled nuclear reactors and serpentine boilers.

The significance of the flow patterns in predicting two-phase flow parameters has been discussed by several investigators (Wallis 1969; Hewitt & Hall-Taylor 1970; Taitel *et al.* 1980; Hewitt 1982). Considerable advances have been made in modeling flow pattern transitions in circular tubes (Dukler & Taitel 1986). There is, however, a lack of experimental data on flow patterns in an annulus. Sadatomi *et al.* (1982) suggested a flow pattern map for different conduit cross-sectional shapes, including a concentric annulus, but provided no information on the factors affecting the flow pattern transitions. This study examines these factors and proposes models to predict the transitions. Since most of the reported data on flow patterns have been derived by direct visual observations, which is largely subjective, part of this study focuses on developing a more objective flow pattern identification method.

EXPERIMENTAL SYSTEM

The schematic diagram of the experimental facility is shown in figure 1. The test section consisted of two acrylic tubes, which are electrically non-conducting, the inner tube having an o.d. of 0.0508 m and the outer tube with an i.d. of 0.0762 m. The column length from the point of the air injection to the top of the column was 6.93 m.

The inner tube could be moved with the help of four sets of spacers (denoted by S in figure 1) so that any degree of eccentricity could be achieved. Air was supplied at 690 kPa from a central compressed air line. The incoming air was filtered, regulated to the desired pressure and measured through rotameters or an orifice meter. The air injection system, located at a distance of 0.076 m from the bottom of the column, consisted of either four or eight polyethylene tubes (0.0127 m dia). Needle valves were used on each of the four tubes for low gas flow rates to maintain constant flow, while for high gas flow rates the needle valves were removed and eight injectors were used instead

†Present address: Anadrill Schlumberger, Sugarland, TX 77478, U.S.A.
‡To whom all correspondence should be addressed.

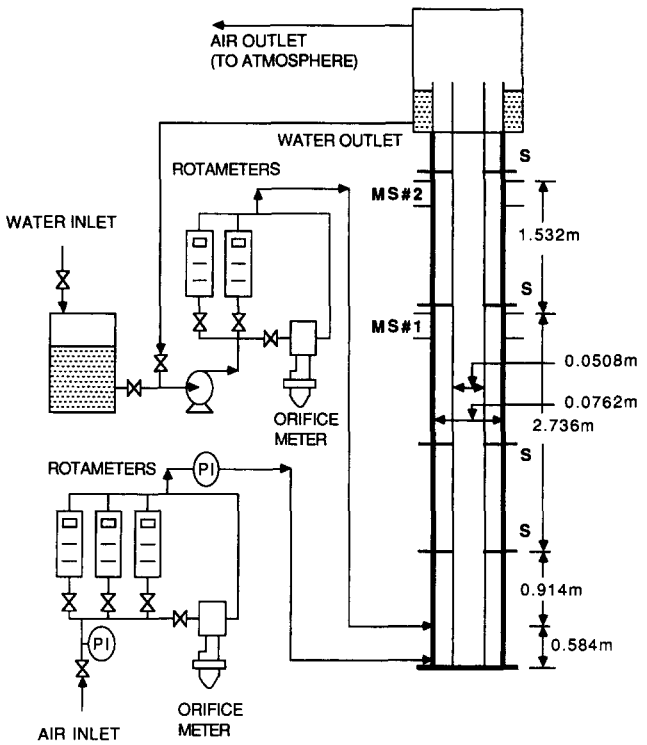

Figure 1. The flow loop. MS = measuring station, S = spacer.

of four. Water was introduced radially through eight ports (0.0127 m dia) at a distance 0.508 m above the air injectors. Water and air flowed up the annulus and discharged into an overhead separator. Air was vented to the atmosphere while water was circulated through the system in a closed cycle by means of a centrifugal pump.

Flow pattern identification was accomplished by the conductance probe method originally proposed by Solomon (1962) and Griffith (1964) and improved by Barnea *et al.* (1980). The adaption of this idea to the annular configuration is shown in figure 2 which shows the peripheral location of the conductance probes. Probes A and C were made of silver-plated copper-clad steel wire (0.3 mm dia), Teflon-coated with an o.d. of 0.97 mm, having only the tip electrically exposed to the two-phase mixture. Both probes were movable so that the tip could be adjusted near the center of the gap. Probes B and D, made of stainless steel wire (0.3 mm dia), were fixed and mounted flush with the inside wall of the outer tube and the outside wall of the inner tube, respectively, and located 180° apart around the perimeter. Two grounds were utilized, probes 1E and 2E (0.0127 m dia) mounted flush on the inner and outer tubes, respectively. A power supply provided variable d.c. voltage. Current flow between each probe and either ground was passed through a fixed resistor and the resulting time-varying voltage drop was the signal of interest. For example, the presence of liquid in the space between probes A and 1E would give a high voltage reading, V_A, while an air gap covering probe A would give zero voltage. The conductance probe measurements were carried out at two axial locations along the test section, indicated as MS # 1 and MS # 2 in figure 1. The probe plane was 0.0508 m below the top of each measuring station. Details of the equipment are given in Kelessidis (1986).

FLOW DESCRIPTION

In gas–liquid flows, the two phases may distribute in a number of geometrical configurations depending on the flow rates, shape and size of the conduit, inclination and fluid properties. Visual observations indicate that natural groupings or patterns exist for which the spatial distribution of the two phases is more or less the same. The flow patterns observed in vertical concentric or

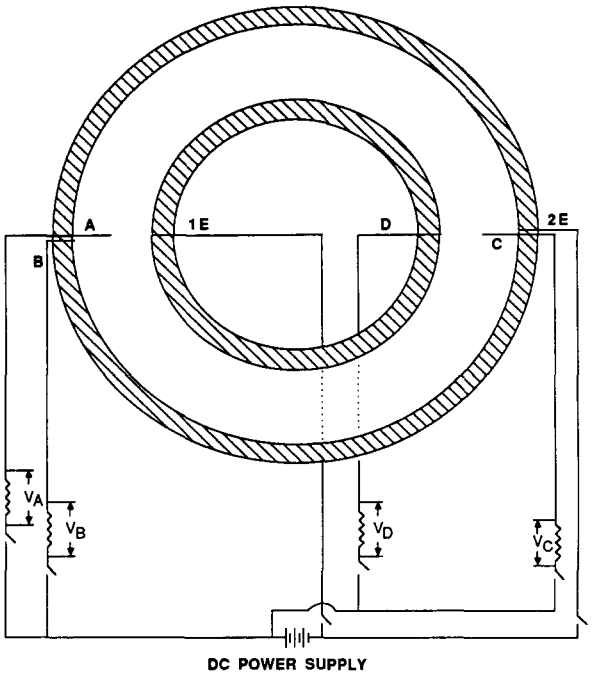

Figure 2. Schematic diagram of the conductivity probes.

eccentric annuli are similar to those seen in round tubes. These four basic flow patterns are pictured in figure 3:

Bubble flow. The gas phase is distributed in the continuous liquid phase in the form of discrete bubbles.

Slug flow. Gas flows mainly in large bubbles designated as "Taylor bubbles". There is a difference between the Taylor bubbles observed in an annulus and those observed in round tubes. The latter are bullet shaped, with a diameter almost equal to the pipe diameter, moving upward essentially axisymmetrically. Taylor bubbles in an annulus are wrapped around the inner tube. Liquid falls downwards in the space between the Taylor bubble and the walls of the annulus as well as in the peripheral area not occupied by the Taylor bubble. In the latter case, the liquid carries distributed bubbles. The liquid flows upwards in the liquid slugs which separate the Taylor bubbles, bridging the annulus and carry distributed bubbles.

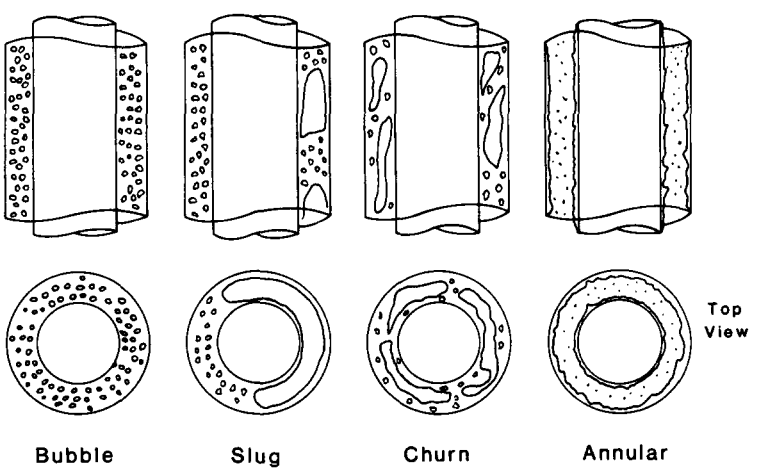

Figure 3. Schematic representations of flow patterns for upward two-phase flow in a concentric annulus.

Churn flow. This distribution has similar characteristics to slug flow but is more chaotic. The gas is moving continuously upwards lifting the liquid to a certain height. The liquid then falls, accumulates, bridges the two tubes of the annulus and is lifted up by the gas again. This chaotic oscillatory motion of the liquid is characteristic of churn flow.

Annular flow. Liquid flows upwards as a film on the walls of both the inner and the outer tube, while the gas flows upwards in the annular space between the liquid films carrying liquid droplets. At very high gas and liquid flow rates large concentrations of droplets exist in the gas core. The droplets tend to agglomerate and coalesce forming large lumps of frothy two-phase mixture. This condition, a subset of the annular flow pattern, is designated as annular flow with lumps.

Transition between patterns is never sharply defined. As the flow rates are changed and the patterns start changing, one observes features of the flow which may be characteristic of two patterns. In this work attempts have been made to define these transition zones.

FLOW PATTERN IDENTIFICATION

Classification of the flow patterns was accomplished using probability density function (PDF) analysis of the voltage–time traces obtained from the conductance probes. Consider a voltage–time trace signal $V(t)$, where the voltage scale is divided into equal increments of width w and the time scale into equal increments of width ΔT (figure 4). If during the observation period T the voltage is seen within the range $(v - w/2, v + w/2)$ for a total of n_i times, then, for a stationary time series, the PDF, $p(v)$, is defined as

$$p(v) = \lim_{w \to 0} \frac{P[v, w]}{w} = \lim_{w \to 0} \frac{1}{w} \left(\lim_{T \to \infty} \frac{T_x}{T} \right), \qquad [1]$$

where $P[v,w]$ is the probability distribution function and $T_x = n_i \Delta T$. The data taken for the flow pattern identification was proved stationary by applying the RUN TEST (Bendat & Piersol 1971). The time interval ΔT for this study was 1 ms. Plots of the PDF of the measured voltage from probes A or C to either ground could be expected to display the following characteristics:

Bubble flow. The probe tip will be exposed primarily to liquid and little gas. Hence, the PDF plot will show a distribution with a single peak near the maximum voltage values (figure 5).

Slug flow. The probe will encounter either all gas, as the Taylor bubble passes, or a bubbly mixture in the presence of liquid. The PDF should therefore be bimodal with one peak essentially at zero voltage and another peak at a high voltage, as in bubble flow (figure 6).

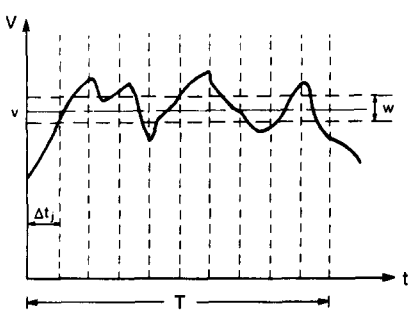

Figure 4. Voltage–time trace to illustrate the estimation of the PDF, $p(v) = \lim_{\substack{w \to 0 \\ T \to 0}} (n_i \Delta T / T w)$.

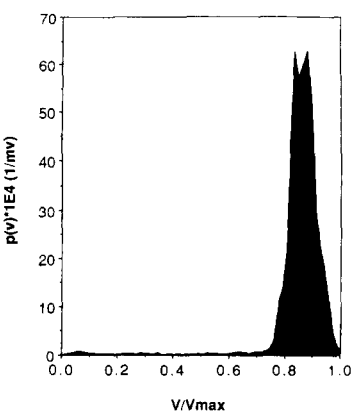

Figure 5. PDF plot for bubble flow. $U_{LS} = 0.01$ m/s, $U_{GS} = 0.03$ m/s, $V_{max} = 1340$ mV.

Annular flow. The voltage signal is always zero. Therefore, a single peak at zero is expected (figure 10).

Characterizing these three flow patterns using PDF analysis of conductivity probe signals is similar to that proposed by Jones & Zuber (1976) for X-ray beam attenuation. However, when visual access is possible such a qualitative description of the PDF curves simply replaces the even more qualitative visual description of the flow itself. While well-established patterns are easy to identify either visually or from PDF curves, the transition between the patterns is not clear. A more quantitative basis for determining when transition is taking place, as indicated by the data, is suggested here from the analysis of the PDF data.

In what follows typical PDF plots are presented for each flow pattern and flow pattern transition. PDF is plotted vs V/V_{max}, where V_{max} is the maximum value of the voltage for which a non-zero PDF value is estimated. The plots were prepared from signals taken by probe C with ground 1E. Similar behavior was observed for probe C with ground 2E as well as for probe A with either ground for the concentric annulus. The results from probe A with ground 1E were slightly different for the eccentric annulus for reasons discussed later. Probes B and D did not reveal any significant information regarding the flow patterns. Based on the signals from both probes, however, it was evident that there was always a liquid film both on the inner and outer tubes of the annulus when a Taylor bubble was present, as well as in annular flow. This information was then utilized in deriving the mathematical models describing the flow pattern transitions.

Bubble flow

A single peak exists at V/V_{max} near 1.0 such that $\int p\, dv = 1$ for $V/V_{max} > 0.75$ (figure 5).

Slug flow

Two well-defined peaks exist, one in the range of $0.75 \leqslant V/V_{max} \leqslant 1.0$ and one which has a maximum at zero. For well-established slug flow to exist we suggest that Taylor bubbles must occupy at least 20% of the length of the column. Thus, the peak at low voltage values ($V/V_{max} \leqslant 0.25$) must have an integral > 0.2 (figure 6).

Bubble–slug transition

If the PDF is bimodal but the integral under the peak at low voltage values is < 0.2, the pattern is characterized as one of transition between the bubble and the slug flow patterns (figure 7).

Churn flow

The PDF displays a single peak again but now it is located at low voltages with its maximum at zero. The peak in the range $0.75 \leqslant V/V_{max} \leqslant 1.0$, which is characteristic of coherent liquid slugs, has disappeared. However, one always observes low but non-zero PDF at high voltages which indicate liquid bridging (figure 8).

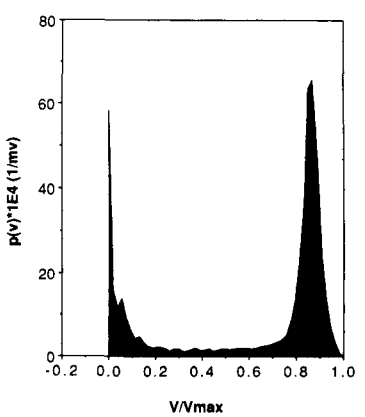

Figure 6. PDF plot for slug flow. $U_{LS} = 0.01$ m/s, $U_{GS} = 0.15$ m/s, $V_{max} = 1080$ mV.

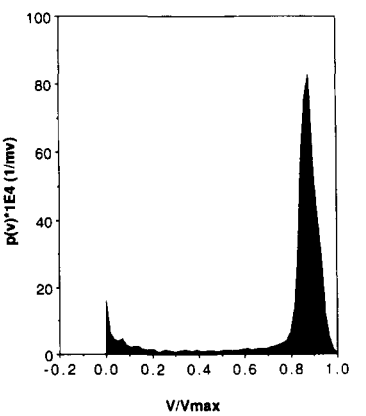

Figure 7. PDF plot for the transition from bubble to slug flow. $U_{LS} = 0.01$ m/s, $U_{GS} = 0.05$ m/s, $V_{max} = 1180$ mV.

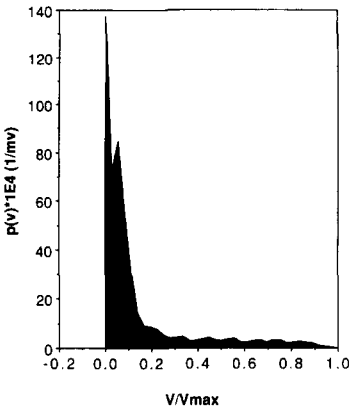

Figure 8. PDF plot for churn flow. $U_{LS} = 0.01$ m/s, $U_{GS} = 3.82$ m/s, $V_{max} = 720$ mV.

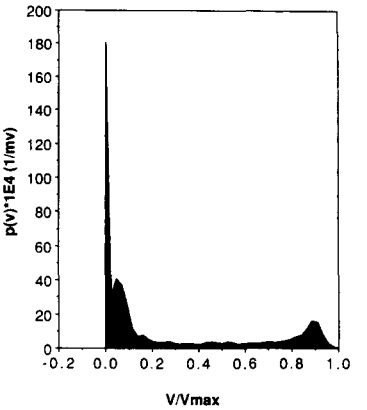

Figure 9. PDF plot for the transition from slug to churn flow. $U_{LS} = 0.01$ m/s, $u_{GS} = 1.72$ m/s, $V_{max} = 880$ mV.

Slug–churn transition

With the concept that for slug flow to exist, the liquid slugs carrying gas bubbles must be present over at least 20% of the length of the column, we characterize this transition as one where the peak at high voltages which existed for slug flow can still be observed but its integral is now <0.2 (figure 9).

Annular flow

Since the probe output is zero voltage, one observes a single peak at this voltage (figure 10).

Churn–annular transition

A condition is characterized as transition from churn to annular flow when there is some distribution of the PDF at low values of the voltage ($V/V_{max} \leqslant 0.25$), but the most probable value is zero and hence a large peak at zero voltage is observed (figure 11).

Annular flow with lumps

This distribution is characterized by the appearance of frothy aerated liquid at high gas and liquid flow rates. There is occasional bridging between the two tubes of the annulus but the void fraction is high, resulting in a very low amplitude voltage signal. The PDF therefore exhibits a single peak, not at zero, but at low voltage ($<0.5V_{max}$) (figure 12).

Churn–annular with lumps transition

The PDF displays the characteristics of both flow patterns. A single peak is observed at low voltage but there is also a low but non-zero PDF at high voltage values (figure 13).

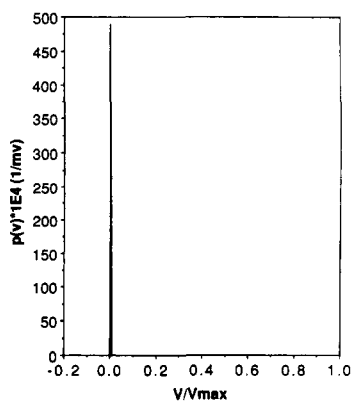

Figure 10. PDF plot for annular flow. $U_{LS} = 0.01$ m/s, $U_{GS} = 14.65$ m/s, $V_{max} = 80$ mV.

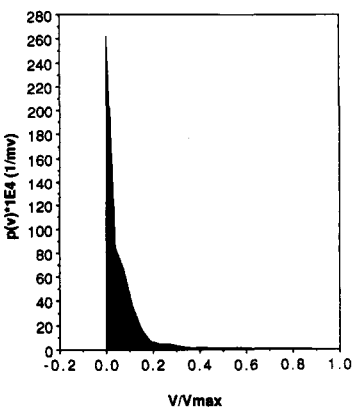

Figure 11. PDF plot for the transition from churn to annular flow. $U_{LS} = 0.01$ m/s, $U_{GS} = 9.03$ m/s, $V_{max} = 540$ mV.

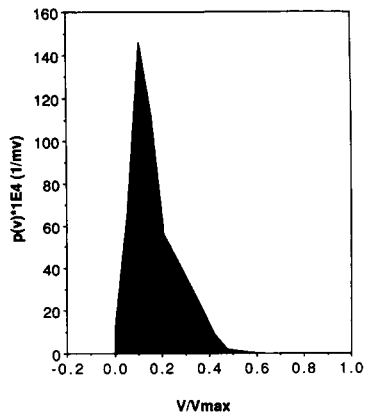

Figure 12. PDF plot for annular flow with lumps. $U_{LS} = 1.16$ m/s, $U_{GS} = 14.7$ m/s, $V_{max} = 380$ mV.

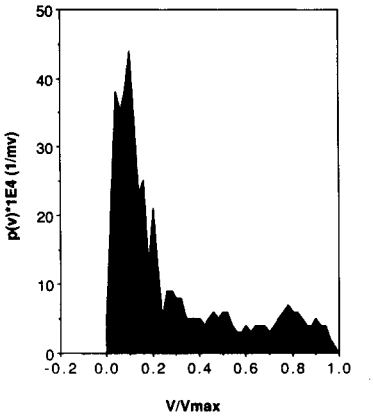

Figure 13. PDF plot for the transition from churn to annular flow with lumps. $U_{LS} = 1.16$ m/s, $U_{GS} = 3.6$ m/s, $V_{max} = 720$ mV.

EXPERIMENTAL RESULTS

Data was taken at the two measuring stations over a range of gas (0.0001–0.0851 kg/s) and liquid (0.019–4.680 kg/s) flow rates and the data classified as to the flow pattern using the criteria discussed above. Flow pattern maps were then constructed for the concentric and the eccentric annulus at both measuring stations. Typical results are presented in figures 14 and 15 for the concentric and the eccentric annulus, respectively, both at measuring station 1. In the eccentric annulus the probe was located on the wide side. The eccentricity, defined as the ratio of the distance between the axes of the tubes to the gap width of the concentric annulus, was 50%.

Analysis of the experimental results indicated that the closeness of the measuring station to the discharge location does not have any significant effect on the flow pattern transitions and the differences observed are within experimental error [figures 16(a, b)]. The degree of eccentricity has little effect on the flow pattern transitions and results in delayed local behavior associated with particular flow patterns on the narrow side of the annulus compared to the wide one. For example, for any liquid rate, the transition from bubble to slug flow is detected to take place at lower gas rates on the wide side. That is, when Taylor bubbles first make their appearance they travel predominantly on the wide side with the narrow side giving the appearance of bubbly flow. As the gas rate is increased, the regular occurrence of Taylor bubbles is observed on the narrow side as well. The delay is characteristic of all transitions. When the gas rate is increased and annular flow

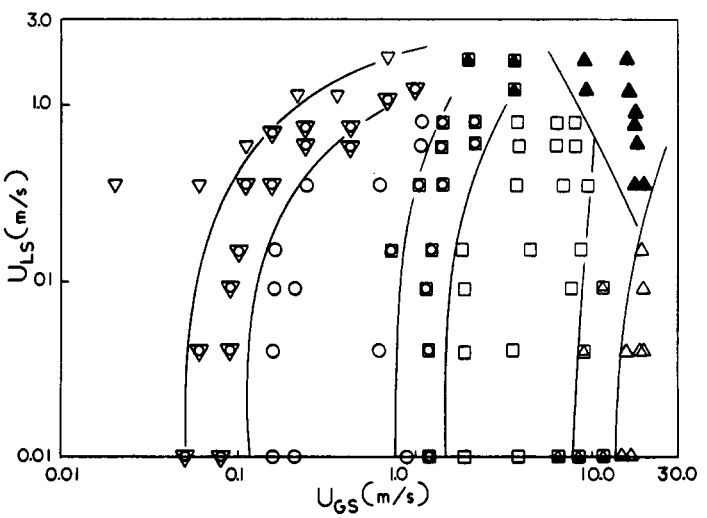

Figure 14. Flow pattern map. PDF analysis of time traces. MS # 1; concentric annulus. ▽, Bubble flow; ○, slug flow; □, churn flow; △, annular flow; ▲, annular flow with lumps.

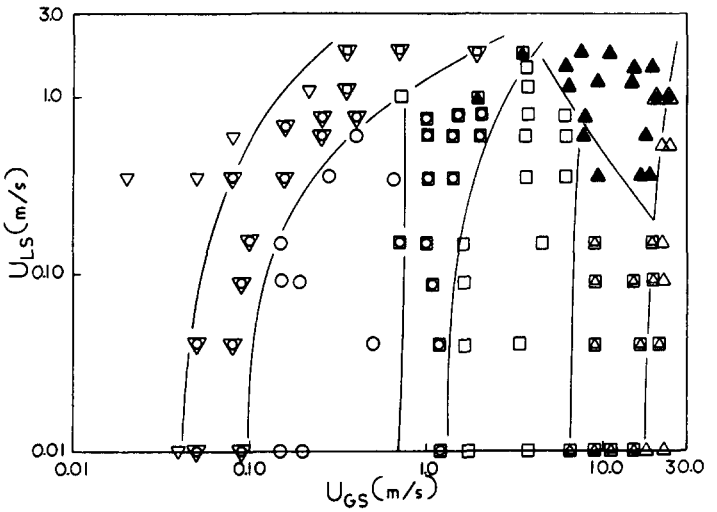

Figure 15. Flow pattern map. PDF analysis of time traces. MS # 1; eccentric annulus. Key as in figure 14.

is first established on the wide side, the condition on the narrow side is still one of churning. These results were evident from the comparison of the flow pattern map derived from PDF analysis of the signal taken from probe A with probe 1E vs that from probe C with probe 2E.

MATHEMATICAL MODELS FOR THE FLOW PATTERN TRANSITIONS

The transition criteria which will be developed are based largely on the ideas presented by Taitel *et al.* (1980).

A. Concentric Annulus

Bubble–slug flow transition

Low liquid flow rates. Visual observations indicate that bubble flow in an annulus has similar characteristics to that in round tubes. As the gas flow rate is increased (at low liquid flow rates) the bubble density increases. At these low liquid flow rates the bubbles rise vertically in a zig-zag motion occasionally colliding to form larger bubbles. A point is reached where the discrete bubbles become so closely packed that many collisions occur and the rate of agglomeration to form larger bubbles increases sharply. This results in the transitions to slug flow.

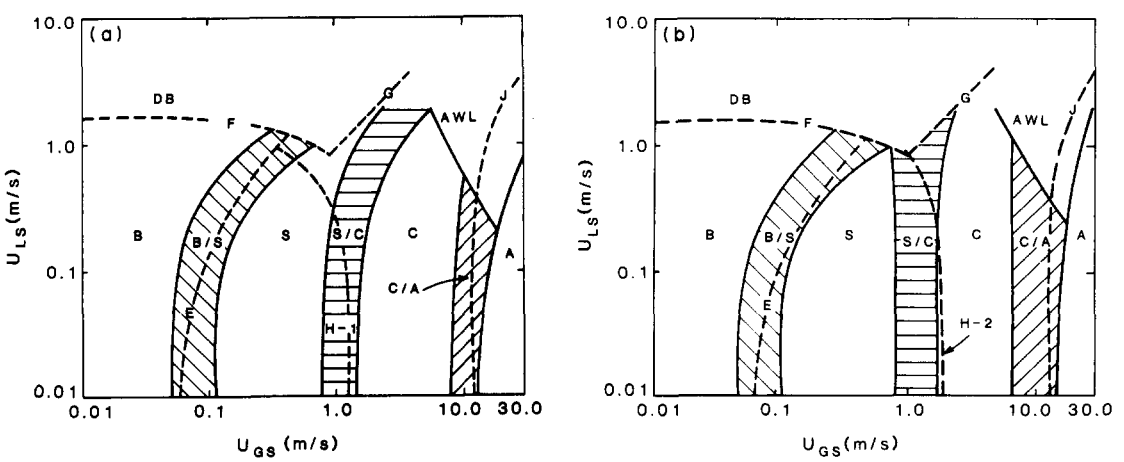

Figure 16. Comparison of predicted and experimental flow pattern transition boundaries in a concentric annulus: (a) MS # 1; (b) MS # 2.——, Experiment; – – –, theory; ▨, mixed flow patterns.

Experimental evidence indicates that the transition from bubble to slug flow occurs at values of the void fraction ranging from 0.25 to 0.30 (Griffith & Synder 1964). Radovcich & Moisis (1962) provided a semi-theoretical approach postulating that the transition takes place when the frequency of collisions of the discrete bubbles is very high. It was shown that this happens at a void fraction around 0.30. Taitel *et al.* (1980) derived a value of 0.25. They assumed the bubbles to be spherical and arranged in a cubic lattice. Therefore, the maximum allowable packing occurs at a void fraction of 0.52. They stipulated, however, that the closest distance between the bubbles before transition must be one which permits some freedom of motion for each individual bubble. If this spacing is assumed to be approximately half the radius of the bubbles, this corresponds to about 25% voids.

Based on the above mechanism, the geometry of the channel does not enter into the derivation for the value of the void fraction at the transition of bubble to slug flow. Venkateswararao *et al.* (1982) used similar arguments to derive the value of 0.25 for the transition from bubble to slug flow in a rod bundle. Their model compared well with their experimental data. It is assumed, therefore, that at liquid flow rates low enough, such that bubble breakup due to turbulence is small, the transition from bubble to slug flow in a concentric annulus takes place when the void fraction averaged over the flow cross-section reaches the value of 0.25.

If the gas bubbles rise with the velocity U_G, this velocity is related to the superficial gas velocity, U_{GS}, by

$$U_{GS} = \epsilon U_G, \qquad [2]$$

where ϵ is the void fraction. Similarly, the average liquid velocity, U_L, is related to the superficial liquid velocity, U_{LS}, by

$$U_{LS} = (1 - \epsilon)U_L. \qquad [3]$$

If U_0 is the rise velocity of the bubbles relative to the liquid,

$$U_G = U_L + U_0. \qquad [4]$$

In this model, radial variations are ignored and U_G and U_L are assumed equal to the area average velocities. At low liquid rates, the bubbles are large enough, so that the rise velocity is independent of the bubble size and depends only on the physical properties of the two phases. Harmathy (1960) indicated that for a single bubble rising in an infinite medium, the rise velocity $U_{0\infty}$ is given by

$$U_{0\infty} = 1.53\left[\frac{g(\rho_L - \rho_G)\sigma}{\rho_L^2}\right]^{1/4}, \qquad [5]$$

where ρ_G and ρ_L are the gas and liquid densities, respectively, g is the acceleration due to gravity and σ is the surface tension. Zuber & Hench (1962) indicated that for a bubble rising in a swarm of bubbles, the correct velocity U_0 should be given by

$$U_0 = (1 - \epsilon)^{1/2} U_{0\infty}. \qquad [6]$$

Equations [2]–[6], when combined, yield

$$U_{LS} = U_{GS}\frac{(1-\epsilon)}{\epsilon} - 1.53(1-\epsilon)^{3/2}\left[\frac{g(\rho_L - \rho_G)\sigma}{\rho_L^2}\right]^{1/4}. \qquad [7]$$

Letting $\epsilon = \epsilon_T = 0.25$ for the transition from bubble to slug flow, [7] becomes

$$U_{LS} = 3.0U_{GS} - \left[\frac{g(\rho_L - \rho_G)\sigma}{\rho_L^2}\right]^{1/4}. \qquad [8]$$

Once the fluid properties are set, [8] will give the locus of the points at which the transition from bubble to slug flow takes place in a concentric annulus. For an air–water system at 25°C and a pressure of approx. 10^5 N/m^2, [8] gives curve E, shown as the dotted line in figures 16(a,b). The solid lines represent the boundaries of the experimental data for both measuring stations. Good agreement is observed between the theory and experiments for both measuring locations. The fact that there is a transition zone shown by the experimental data indicates that the transition to slug flow starts at a void fraction somewhat less than 0.25 and ends at a value slightly higher than 0.25,

in accordance with the observations reported for the transition in circular tubes which were discussed above.

High liquid flow rates. At high liquid flow rates, turbulent forces tend to break up any large bubbles and disperse the gas phase. This results in a finely dispersed bubble flow where the void fraction can exceed the value of 0.25 without the transition to slug flow taking place. The maximum stable diameter of a dispersed phase in an immiscible system can be derived from the theory developed by Hinze (1955). This diameter is derived by a force balance between surface tension forces and the forces due to turbulent fluctuations and is given by

$$d_{max} = k\left(\frac{\sigma}{\rho_L}\right)^{3/5}(e_d)^{-2/5}, \qquad [9]$$

where k is a constant and e_d is energy dissipation per unit mass. The experimental data of Clay (1940) indicated a value of $k = 0.725$.

For turbulent flow in an annulus, the rate of energy dissipation per unit mass, e_d, is given by

$$e_d = \left|\frac{dP}{dz}\right|_{fr}\frac{U_M}{\rho_M}, \qquad [10]$$

where $|dP/dz|_{fr}$ is the frictional loss given by

$$\left|\frac{dP}{dz}\right|_{fr} = \frac{2f}{D_h}\rho_M U_M^2, \qquad [11]$$

U_M is the mixture velocity

$$U_M = U_{LS} + U_{GS}, \qquad [12]$$

D_h is the hydraulic diameter

$$D_h = D_2 - D_1, \qquad [13]$$

ρ_M is the mixture density, f is the friction factor and D_2 and D_1 are the diameters of the outer and the inner tube, respectively.

When the bubble size produced by this breakup process is so small that the bubbles move rectilinearly, then coalescence is not expected to take place even if the void fraction exceeds 0.25. This critical size, d_{crit}, is given by Brodkey (1967) as

$$d_{crit} = \left[\frac{0.4\sigma}{(\rho_L - \rho_G)g}\right]^{1/2}. \qquad [14]$$

If $d_{max} \leqslant d_{crit}$, the bubbles will remain spherical, move rectilinearly and the void fraction may exceed 0.25 without the transition to slug flow taking place.

The friction factor may be expressed as a function of the Reynolds number, $Re = U_M D_h/\nu_L$,

$$f = C_f(Re)^{-n}, \qquad [15]$$

where ν_L is the liquid kinematic viscosity and n and C_f are constants. Setting $d_{max} = d_{crit}$, all the above give

$$\left[\frac{0.4\sigma}{(\rho_L - \rho_G)g}\right]^{1/2}\left(\frac{\rho_L}{\sigma}\right)^{3/5}\left[\frac{2}{D_h}C_f\left(\frac{D_h}{\nu_L}\right)^{-n}\right]^{2/5}U_M^{2(3-n)/5} = 0.725. \qquad [16]$$

Interpolation of the data for friction is a concentric annulus of Jonsson & Sparrow (1966) for the diameter ratio used in this study ($D_2/D_1 = 1.5$) gave $C_f = 0.0380$ and $n = 0.18$. For an air–water system at 25°C and a pressure of approx. 10^5 N/m^2, [16] gives for the present system,

$$U_M = U_{LS} + U_{GS} = 1.726 \text{ m/s}. \qquad [17]$$

Equation [17] is shown as curve F in figures 16(a,b). The maximum allowable bubble density is 0.52, if one assumes the bubbles are spherical and arranged in a cubic lattice (Taitel *et al.* 1980). Therefore, curve F terminates at curve G, which relates U_{LS} and U_{GS} for $\epsilon = 0.52$ and is given by

$$U_{LS} = 0.92U_{GS} - 0.08 \text{ m/s}. \qquad [18]$$

Due to limitations in pumping capacity, the maximum superficial liquid velocity that could be achieved was 1.8 m/s, which is below the transition region indicated by curve F. Therefore, this part of the theory could not be tested by comparison with experimental data.

Slug–churn flow transition

Visual observations indicate that churn flow in an annulus is an entrance region phenomenon similar to that observed in round tubes (Taitel *et al.* 1980). Churn flow could be observed in regions close to the two-phase mixture injectors, while stable slug flow was seen to exist at distances farther away from the entrance region.

Taitel *et al.* suggested that churn flow exists when the liquid slug is smaller than a critical, stable slug length. It was shown that this stable slug length is about 16 tube dia. Experimental measurements in round tubes indicate that the ratio of the liquid slug length to the pipe diameter during stable slug flow is essentially constant, although the reported value varies for the different investigators [e.g. Akagawa & Sakaguchi (1966) report a value of 7.5, Taitel *et al.* (1980) report a value of 16, while Fernandes (1981) reports a value of 21.5].

The liquid slug length l_s in the annulus of the present study was measured using two conductance probes. The results are shown in figure 17. There is no systematic variation in the length of the liquid slug with the gas or the liquid flow rates. The average value of all 11 measurements (for both the concentric and the eccentric annulus) is $l_s = 0.53$ m with a standard deviation of $SD_{l_s} = 0.08$ m, thus giving a dimensionless liquid slug length of

$$\frac{l_s}{D_h} = 20.7. \qquad [19]$$

It is proposed that the stability of the liquid slug in an annulus is associated with the liquid falling as a film around the Taylor bubble. There may be an effect of the liquid falling in the peripheral area not occupied by the bubble, but this is not considered in the following analysis. It is assumed that the liquid films falling around the inner and outer tubes can be considered as cylindrical wall jets. It can be shown (Rajaratnam 1976) that under the condition of $b_m/R_1 \ll 1$, the cylindrical wall jet is behaving like a wall jet, where b_m is the normal distance from the cylinder to the point where the velocity is half the maximum velocity and R_1 is the radius of the cylinder. This condition holds for both the inner and the outer films, since the film thickness is very small. For plane wall jets, the velocity distribution has been found to be similar by Myers *et al.* (1963) and Schwarz & Cosart (1961), as reported by Rajaratnam (1976). Rajaratnam reports on the work of Verhoff (1963) who proposed an empirical expression which describes the similarity curve

$$\frac{u_j}{u_{mj}} = 1.4794 y_b^{1/7}[1 - \mathrm{erf}(0.67758 y_b)], \qquad [20]$$

where $y_b = y/b_m$, u_j is the jet velocity at some point (z, y), z is the axial coordinate, y is the radial distance from the wall and u_{mj} is the maximum jet velocity located at some distance from the plane wall. Experimental evidence indicates that

$$b_m = 0.068z. \qquad [21]$$

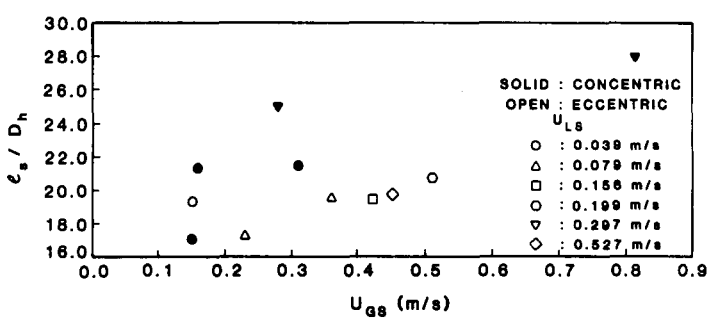

Figure 17. Dimensionless liquid slug length vs U_{LS} and U_{GS} for slug flow in an annulus.

It is proposed here that the liquid slug is stable if it is long enough so that the jet has been absorbed by the fluid and the velocity has slowed down to that of the surroundings. Hence, one searches for the conditions under which

$$\frac{u_j}{u_{mj}} \to 1;\ y \to \frac{D_2 - D_1}{4};\ z \to l_s.$$

Equation [20] shows that the above conditions are satisfied when

$$\frac{l_s}{D_h} = 22.4. \qquad [22]$$

The above result is close to the experimental value, [19], despite the assumptions in the derivation, namely:

(1) The liquid is confined and not of infinite extent.
(2) The jet is cylindrical and not a wall jet.
(3) The jet is discharging in a moving liquid stream (compound jet) and not in a stagnant pool of liquid.

Since there are no additional data available on continuous slug flow in an annulus, no further check of [22] could be made. It should be noted that Taitel *et al.* (1980) used a similar approach to derive the value of $l_s/D = 16$. The difference is that they modeled the liquid film as a free jet—which may be justified for flow in round tubes but not for flow in an annulus, because the gap size is generally small and furthermore, there are two liquid films present which merge to the center of the gap thus the films can no longer be modeled as free jets.

The entry length required for the establishment of stable slug flow is determined according to the overtaking model proposed by Taitel *et al.* (1980). Consider two Taylor bubbles rising in a concentric annulus (figure 18). The top one is moving with a constant velocity U_N, while the second one is rising with a velocity U_G. Experimental evidence (Kelessidis 1986) indicates that during stable slug flow, the rise velocity of Taylor bubbles is correlated to the mixture velocity U_M by

$$U_N = CU_M + U_{RC}, \qquad [23]$$

where U_{RC} is the bubble rise velocity in a stagnant liquid in a concentric annulus, having the value of $U_{RC} = 0.370$ m/s for the annulus in this study, while C is a constant having the value of $C = 1.55$. Kelessidis has also shown that the bubble nose is asymmetric and speculated that the liquid velocity ahead of the bubble tip U_t has the value

$$U_t = CU_M. \qquad [24]$$

An exponential variation of the liquid velocity is assumed from the value of U_N at $z = 0$ to the value of CU_M at $z = l_s$:

$$U_t = U_N \exp\left(-\frac{\beta z}{l_s}\right) + CU_M\left[1 - \exp\left(-\frac{\beta z}{l_s}\right)\right], \qquad [25]$$

where β is a constant which characterizes the decay rate. Taitel *et al.* used the value of $\beta = 4.6$ so that the decay rate at $z = l_s$ would be 99%, while for this study a decay rate of 99.9% was chosen so that somewhat better agreement with the experiments could be achieved. This results in a value of $\beta = 7$. If the liquid slug is short, the trailing bubble accelerates and its velocity, U_G, is given by

$$U_G = U_t + U_{RC}. \qquad [26]$$

The approach velocity is therefore given by

$$-\frac{dz}{dt} = U_G - U_N = U_{RC} \exp\left(-\frac{\beta z}{l_s}\right). \qquad [27]$$

Following Taitel *et al.* (1980), the entrance length is estimated as follows: it is assumed that during the coalescence of two slugs, a new slug of double the length is created. The entrance length will extend up to the point where the length of the new slug formed during the coalescence period,

l_L, will be $l_s/2$, since the merger of the last two slugs will be quite slow. Integration of [27] gives the time needed for the formation of a bigger slug. Summation of all the individual times and multiplication by U_N yields the estimated entrance length l_E,

$$l_E = \frac{l_s U_N}{\beta U_{RC}} \sum_{i=0}^{\infty} \left[\exp\left(\frac{\beta l_{L_i}}{l_s}\right) - 1 \right] \quad [28]$$

where l_{L_i} takes the values $\ldots l_s/16, l_s/8, l_s/4$. Using $\beta = 7$ and $l_s = 22.4 D_h$, [28] becomes

$$\frac{l_E}{D_h} = 22.96 \left(C \frac{U_M}{U_{RC}} + 1 \right). \quad [29]$$

The solution of [29] for the annulus in this study is shown in figures 16(a,b) as curves H-1 and H-2 corresponding to the two measuring stations, namely for MS # 1, $l_E/D_h = 142$, $U_M = 1.24$ m/s; and for MS # 2, $l_E/D_h = 202$, $U_M = 1.86$ m/s. Comparison of theory with the experimental results shows good agreement for both measuring stations.

Churn–annular transition

It is proposed that the transition from churn to annular flow occurs when the void fraction for churn flow, ϵ_{Ch} and the void fraction for annular flow, ϵ_A, are equal. A similar mechanism has been proposed by Venkateswararao *et al.* (1982) for this transition in a rod bundle.

Let δ_1 and δ_2 denote the liquid film thickness on the outer surface of the inner tube and the inner surface of the outer tube, respectively (figure 19), during annular flow. To effectively close the problem it is assumed that $\delta_1 \approx \delta_2 = \delta$. The gas flow area A_G is given by

$$A_G = \frac{\pi}{4}[(D_2 - 2\delta)^2 - (D_1 + 2\delta)^2]. \quad [30]$$

Hence, the void fraction for annular flow ϵ_A is given by

$$\epsilon_A \equiv \frac{A_G}{A_t} = 1 - \frac{4\delta}{D_2 - D_1}, \quad [31]$$

where A_t is the total cross-sectional area. Consider a differential element of the gas core of length Δz. A force balance, in the absence of acceleration, gives

$$\frac{dP}{dz} + \rho_G g + \frac{P_{1G}\tau_{1i} + P_{2G}\tau_{2i}}{A_G} = 0, \quad [32]$$

where P_{1G} and P_{2G} are the wetted perimeters at the gas–liquid interfaces, given by

$$P_{1G} = \pi(D_1 + 2\delta) \quad [33]$$

and

$$P_{2G} = \pi(D_2 - 2\delta), \quad [34]$$

and τ_{1i} and τ_{2i} are the interfacial shear stresses. If one assumes that the gas velocity is much larger than the liquid velocity, which is true at these high gas flow rates, the interfacial shear stresses are given by

$$\tau_{ji} = \tfrac{1}{2} f_{ji} \rho_G U_G^2, \qquad j = 1, 2, \quad [35]$$

where f_{ji} is the interfacial friction factor. The gas velocity is related to the void fraction by

$$U_{GS} = \epsilon_A U_G. \quad [36]$$

Wallis (1969) gives an empirical expression for the interfacial friction factor in annular flow in a pipe of diameter D,

$$f_i = 0.005 \left(1 + 300 \frac{\delta}{D} \right). \quad [37]$$

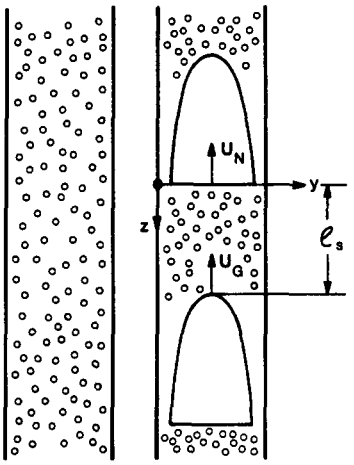

Figure 18. Slug flow geometry.

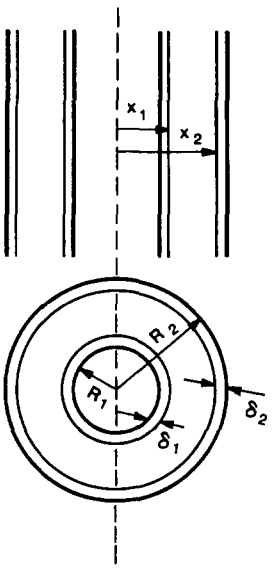

Figure 19. Annular flow geometry.

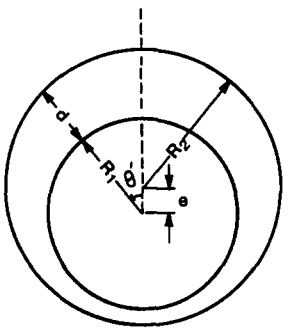

Figure 20. Plan view of the eccentric annulus.

It is proposed that [37] can be used for flow in an annulus provided that D is replaced by D_1 and D_2 for the inner and the outer tubes, respectively. Combination of [31]–[37] yields

$$\frac{dP}{dz} - \rho_G g + \frac{0.01\rho_G U_{GS}^2}{\epsilon_A^3(D_2+D_1)}\left[\frac{D_2+D_1}{D_2-D_1} + 150(1-\epsilon_A) + 37.5(1-\epsilon_A)^2\frac{(D_2-D_1)^2}{D_1D_2}\right] = 0. \quad [38]$$

An overall force balance over the segment Δz gives

$$\frac{dP}{dz} + [\epsilon_A\rho_G + (1-\epsilon_A)\rho_L]g + \left(-\frac{dP}{dz}\right)_{fr} = 0, \quad [39]$$

where $-(dP/dz)_{fr}$ represents the frictional losses. These losses can be estimated by performing an integral analysis, similar to the one suggested by Wallis (1969) for annular flow in pipes. This analysis relates the wall shear stress to an assumed velocity profile by means of single-phase correlations which are well-established.

Suppose there is single-phase liquid flow in an annulus with mean velocity $\bar{U}$. The frictional pressure drop is given by

$$\left(-\frac{dP}{dz}\right)_{fr} = \frac{1}{2} f \frac{\rho_L \bar{U}^2}{D_h}. \quad [40]$$

Suppose now that only part of the annulus is occupied by the liquid (figure 19). It can be shown that

$$x_1 = \frac{R_1+R_2}{2} + \frac{\epsilon_A(R_1-R_2)}{2} \quad [41]$$

and

$$x_2 = \frac{R_1+R_2}{2} + \frac{\epsilon_A(R_2-R_1)}{2}. \quad [42]$$

Let u_1 and u_2 denote the point velocities in the liquid films. The superficial liquid velocity U_{LS} is given by

$$U_{LS} = \frac{4}{\pi(D_2^2-D_1^2)}\left(\int_{R_1}^{x_1} 2\pi r u_1\, dr + \int_{x_2}^{R_2} 2\pi r u_2\, dr\right). \quad [43]$$

We assume that the two velocity profiles follow a power law,

$$\frac{u_1}{U_{max}} = \left(\frac{r - R_1}{R_m - R_1}\right)^{1/n} \quad [44]$$

and

$$\frac{u_2}{U_{max}} = \left(\frac{R_2 - r}{R_2 - R_m}\right)^{1/n}, \quad [45]$$

where U_{max} is the maximum liquid velocity and R_m is the point of maximum velocity which coincides with the point of zero shear stress, given by (Kays & Leung 1963)

$$R_m = \frac{D_2}{2} \frac{\left(\frac{D_2}{D_1}\right) + \left(\frac{D_1}{D_2}\right)^{0.343}}{1 + \left(\frac{D_1}{D_2}\right)^{0.343}}. \quad [46]$$

Calculation of the average velocity $\bar{U}$ for a value of $n = 7$ gives $\bar{U}/U_{max} = 0.874$. Knudsen & Katz (1979) report that experimental data for single-phase flow in annuli shows that $\bar{U}/U_{max} = 0.876 \pm 0.02$, in agreement with the above calculated value. Combination of [41]–[45] gives

$$U_{LS} = J(\epsilon_A)\bar{U}, \quad [47]$$

where

$$J(\epsilon_A) = \frac{2.288}{(R_2^2 - R_1^2)} \left\{ \frac{1}{(R_m - R_1)^{1/7}} \left[\frac{7}{8} R_1 (x_1 - R_1)^{8/7} + \frac{7}{15} (x_1 - R_1)^{15/7} \right] + \frac{1}{(R_2 - R_m)^{1/7}} \left[\frac{7}{8} R_2 (R_2 - x_2)^{8/7} - \frac{7}{15} (R_2 - x_2)^{15/7} \right] \right\}. \quad [48]$$

Equations [47] and [48] relate U_{LS} and ϵ_A for annular flow in an annulus to the average velocity $\bar{U}$ that the liquid would have if it were flowing alone. If U_{LS} and $J(\epsilon_A)$ are known, $\bar{U}$ is obtainable from [47] and the frictional losses can be calculated by [40], if an expression for the friction factor for single-phase flow in an annulus is known. The friction factor is expressed as before,

$$f = C_f \mathrm{Re}^{-n}, \quad [15]$$

where $C_f = 0.0380$ and $n = 0.18$. Substitution for $-(\mathrm{d}P/\mathrm{d}z)_{fr}$ into [39] and elimination of the pressure drop term between [38] and [39] yields

$$(\rho_L - \rho_G)(1 - \epsilon_A)g + \frac{2C_f \rho_L (v_L)^n}{(D_h)^{1+n}} \left(\frac{U_{LS}}{J(\epsilon_A)}\right)^{2-n} - \frac{0.01 \rho_G U_{GS}^2}{\epsilon_A^3 (D_2 + D_1)} \times \left[\frac{D_2 + D_1}{D_2 - D_1} + 150(1 - \epsilon_A) + 37.5(1 - \epsilon_A)^2 \frac{(D_2 - D_1)^2}{D_1 D_2} \right] = 0, \quad [49]$$

where $J(\epsilon_A)$ is given by [48].

It has been shown that for two-phase flow in round tubes, the holdup model for slug flow is still valid in the churn flow region (Fernandes *et al.* 1983), namely

$$\epsilon_{Ch} = \epsilon_{Sl} = \frac{U_{GS}}{U_N}. \quad [50]$$

It is assumed that [50] also holds for flow in an annulus and U_N is given by [23]. Hence, the transition to annular flow in an annulus occurs when

$$\epsilon_{Ch} = \epsilon_A. \quad [51]$$

The locus of the transition points has been found by simultaneous solution of [51], [50], [23], [41], [42], [46], [48] and [49] and is shown as curve J in figures 16(a, b). Good agreement is observed with the experimental data for both measuring stations.

B. Eccentric Annulus

Experimental data derived in this study indicated small variations in the flow pattern transitions between the concentric and the eccentric annulus (eccentricity 50%), although certain details of the flow are different. An analysis will be carried out for the eccentric annulus similar to that performed for the concentric annulus and it will be shown that slight modifications of the theory developed above can predict the effect of eccentricity on the flow pattern transitions.

Bubble–slug flow transition

Low liquid flow rates. Visual observations indicate that at low liquid and gas flow rates, the bubble density is small and the bubbles move preferentially on the wide side of the annulus. As the gas flow rate is increased, the bubble density increases, while only a few bubbles are observed in the narrow gap. Based on these observations, it is suggested that the transition from bubble to slug flow occurs when the void fraction is 0.25 locally. The analysis below estimates the cross-sectional area of the eccentric annulus through which the distributed bubbles are most likely to flow.

It is assumed that the presence of the inner tube does not affect the bubble size distribution during bubble flow. Experimental evidence indicates that typical bubble size distribution is 3–5 mm during bubble flow approaching the transition to slug flow in round tubes. For the purposes of computations, a bubble diameter $d_a = 4$ mm is used. The final results are relatively insensitive to the particular choice of d_a in the range 3–5 mm. The plan view of the cross-sectional area of the eccentric annulus is shown in figure 20. It can be shown that

$$A_{\theta'} = \int_0^{\theta'} (\sqrt{R_2^2 - e^2 \sin^2 \omega} + e \cos \omega)^2 \, d\omega - \theta' R_1^2, \qquad [52]$$

where $A_{\theta'}$ is the cross-sectional area of the sector θ' and e is the distance between the centers of the tubes. It is assumed that the bubbles are spherical and arranged in a cubic lattice and that the closest distance between the bubbles before the transition to slug flow is approximately half their radius. Hence, the smallest value that d can take is $d_m = d_a/8 + d_a + d_a/4 + d_a + d_a/8 = 10$ mm, upon using the value of $d_a = 4$ mm. The annulus gap d is given by (Iyoho & Azar 1981):

$$d = \sqrt{R_2^2 - e^2 \sin^2 \theta'} - R_1 + e \cos \theta'. \qquad [53]$$

For $d = d_m$, [53] gives the maximum value of θ', θ_e, which describes the area of the annulus, A_{θ_e}, available for gas flow, in other words, gas flows mainly through the area defined by $-\theta_e \leqslant \theta' \leqslant \theta_e$. For the annulus of the present study, $\theta_e = 1.93$ rad. Hence, the transition to slug flow takes place when the void fraction reaches the value of 0.25 in the area defined by θ_e. The overall void fraction ϵ_t is calculated by

$$\epsilon_t = \epsilon \frac{A_{\theta_e}}{A_t}, \qquad [54]$$

where ϵ is the local void fraction. Equation [7] still holds since it is based on the overall void fraction. The following procedure is therefore proposed to determine the bubble to slug flow transition in an eccentric annulus (any diameter ratio and eccentricity):

(a) determine θ_e such that

$$\sqrt{1 - \left(\frac{e}{R_2}\right)^2 \sin^2 \theta_e} - \left(\frac{R_1}{R_2}\right) + \left(\frac{e}{R_2}\right) \cos \theta_e = \frac{d_m}{R_2},$$

where $d_m = 10$ mm;

(b) calculate A_{θ_e}/A_t by

$$\frac{A_{\theta_e}}{A_t} = \frac{\displaystyle\int_0^{\theta_e} (\sqrt{R_2^2 - e^2 \sin^2 \omega} + e \cos \omega)^2 \, d\omega - \theta_e R_1^2}{\pi (R_2^2 - R_1^2)};$$

(c) let $\epsilon = \epsilon_T = 0.25$;
(d) calculate $\epsilon_t = \epsilon \times (A_{\theta_e}/A_t)$;
(e) calculate the locus of the points at the transition from bubble to slug flow by

$$U_{LS} = \frac{1-\epsilon_t}{\epsilon_t} U_{GS} - (1-\epsilon_t)^{3/2} \left[\frac{g(\rho_L - \rho_G)\sigma}{\rho_L^2}\right]^{1/4}.$$

For the annulus of this study and for an air–water system at 25°C and a pressure of 10^5 N/m^2, this model gives

$$U_{LS} = 4.08 U_{GS} - 0.22 \text{ m/s} \quad [55]$$

and the solution is shown in figures 21(a,b) as curve E. Good agreement between the theory and experiments is observed for both measuring stations. Comparison of the results for the concentric and the eccentric annulus (figures 16 and 21) shows that the effect of the degree of eccentricity for this transition is minor.

High liquid flow rates. At high liquid rates, smaller size bubbles are produced by the breakup process due to turbulent fluctuations. Hence, the above analysis does not hold and the full flow area of the eccentric annulus can carry bubbles. The same transition criteria, proposed for the concentric annulus, hold also for the eccentric annulus, provided that the friction factor is calculated by

$$f = 0.0342(\text{Re})^{-0.18}, \quad [56]$$

derived from interpolation of the experimental data of Jonsson & Sparrow (1966) for the eccentric annulus in this study. Hence, [16] becomes

$$U_M = U_{LS} + U_{GS} = 1.792 \text{ m/s} \quad [57]$$

and is shown as curve F in figures 21(a, b). Curve F terminates at curve G, which relates U_{LS} and U_{GS} for $\epsilon = 0.52$ and is given by [18], as for the concentric annulus. Comparison of [57] and [17] indicates no significant differences for this transition between the concentric and the eccentric annulus.

Slug–churn flow transition

Experimental results indicate that the degree of eccentricity has a small effect on the bubble rise velocity in a stagnant liquid, while there is no effect on the propagation velocity in slug flow, if the former is taken into account (Kelessidis 1986). The measured rise velocity in a stagnant liquid for the eccentric annulus in this study was found to be $U_{RE} = 0.356$ m/s, while the propagation velocity in slug flow is given by

$$U_N = 1.55 U_M + U_{RE} \text{ m/s}. \quad [58]$$

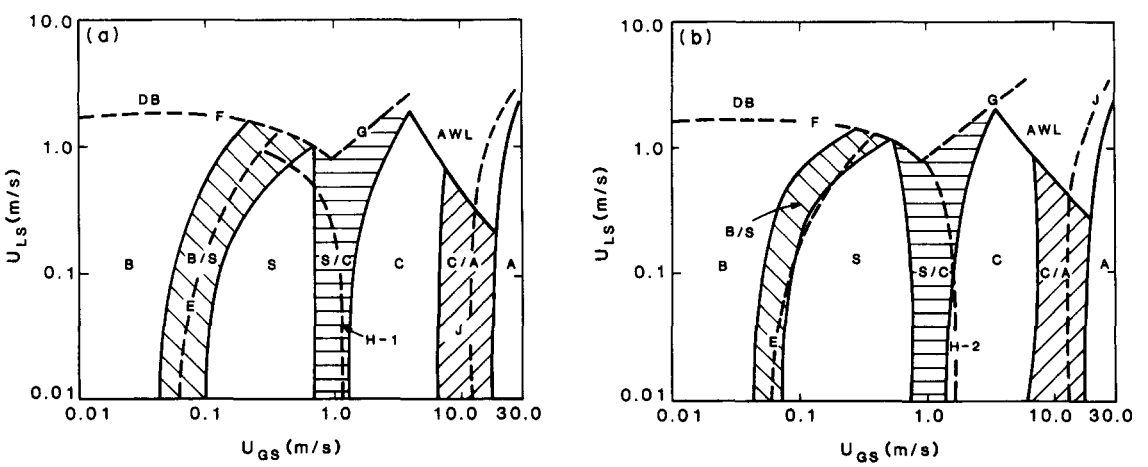

Figure 21. Comparison of predicted and experimental flow pattern transition boundaries in an eccentric annulus: (a) MS # 1; (b) MS # 2. Key as in figures 16(a,b).

The proposed model for the transition from slug to churn flow indicates that the entrance length over which churning may be observed is primarily dependent on U_N. Hence, [29] is shown in figures 21(a,b) as curves H-1 and H-2 corresponding to the two axial locations: $l_E = 142D_h$, $U_M = 1.19$ m/s, and $l_E = 202D_h$, $U_M = 1.79$ m/s, respectively. The agreement with the data may be considered good for both measuring locations.

Churn–annular flow transition

A similar procedure to that followed for the concentric annulus may be used for the eccentric annulus to predict this transition. Departures, however, are expected from the power-law velocity profiles assumed for the velocities in the liquid films, since the velocity varies in the radial as well as in the peripheral direction. It seems, therefore, that a complete solution of turbulent flow in an eccentric annulus would be necessary. If, however, the results for the average liquid velocity, obtained from the analysis for the concentric annulus, are used, the predicted transition from churn to annular flow in the eccentric annulus agrees well with the experimental data. This result is not surprising, since the liquid films are thin and the area over which the velocity profile is integrated is small, so that any errors introduced in the assumed velocity profile do not have a large impact on the final solution. The same procedure was therefore followed, using U_{RE} instead of U_{RC}, and $C_f = 0.0342$. The results are shown as curve J in figures 21(a,b) for the two measuring locations. Good agreement is observed with the experimental results for both measuring stations.

CONCLUSION

Data have been collected which identify flow pattern transitions in a concentric and an eccentric annulus (eccentricity 50%). Criteria have been developed to provide an objective way for the identification of flow patterns as well as of flow pattern transitions, based on PDF analysis of voltage–time traces obtained from conductivity probes. Mathematical models have been developed, based on physical mechanisms suggested for each flow pattern transition, which predict the flow rates for which these transitions take place in concentric annuli. Modifications of the theory to predict the effect of eccentricity on the flow pattern transitions indicate that the degree of eccentricity has a minor effect on the transitions. This is in agreement with the experimental data.

Acknowledgement—This work was supported by Schlumberger-Doll Research.

REFERENCES

AKAGAWA, K. & SAKAGUCHI, T. 1966 Fluctuations of void ratio in two phase flow. *Bull. JSME* **9,** 104–110.

BARNEA, D., SHOHAM, O. & TAITEL, Y. 1980 Flow pattern characterization in two phase flow by electrical conductance probe. *Int. J. Multiphase Flow* **6,** 387–397.

BENDAT, J. S. & PIERSOL, A. G. 1971 *Random Data: Analysis and Measurement Procedures.* Wiley, New York.

BRODKEY, R. S. 1967 *The Phenomena of Fluid Motions.* Addison-Wesley, Reading, Mass.

CLAY, P. H. 1940 The mechanism of emulsion formation in turbulent flow, Part I. *Proc. Acad. Sci. Amsterdam* **43,** 852–865.

DUKLER, A. E. & TAITEL, Y. 1986 Flow pattern transitions in gas–liquid systems. Measurements and modeling. In *Advances in Multiphase Flow,* Vol. 2 (Edited by ZUBER, N., HEWITT, G. F. & DELHAYE, J. M.). McGraw-Hill, New York.

FERNANDES, R. C. 1981 Experimental and theoretical studies of isothermal upward gas–liquid flows in vertical tubes. Ph.D. Dissertation, Univ. of Houston, Tex.

FERNANDES, R. C., SEMIAT, R. & DUKLER, A. E. 1983 Hydrodynamic model for gas–liquid slug flow in tubes. *AIChE Jl* **28,** 981–989.

GRIFFITH, P. 1964 Two phase flow regime detecting. ASME Paper 64-WA/HT-43.

GRIFFITH, P. & SYNDER, G. A. 1964 The bubble–slug transition in a high velocity two phase flow. MIT Report 5003-29 (TID-20947).

HARMATHY, T. Z. 1960 Velocity of large drops and bubbles in media of infinite or restricted extent. *AIChE Jl* **6,** 281–288.

HEWITT, G. F. 1982 Flow regimes. In *Handbook of Multiphase Systems* (Edited by HETSRONI, G.). Hemisphere, Washington, D.C.

HEWITT, G. F. & HALL-TAYLOR, N. S. 1970 *Annular Two Phase Flow.* Pergamon Press, Oxford.

HINZE, J. O. 1955 Fundamentals of the hydrodynamic mechanism of splitting in dispersion processes. *AIChE Jl* **1,** 289–295.

IYOHO, A. W. & AZAR, J. J. 1981 An accurate slot-flow model for non-Newtonian fluid flow through eccentric annuli. *J. Pet. Technol.* **33,** 565–572.

JONES, O. C. & ZUBER, N. 1976 The interrelation between void fraction fluctuations and flow patterns in two phase flow. *Int. J. Multiphase Flow* **2,** 273–306.

JONSSON, V. K. & SPARROW, E. M. 1966 Experiments on turbulent flow phenomena in eccentric annular ducts. *J. Fluid Mech.* **25,** 65–86.

KAYS, W. M. & LEUNG, E. Y. 1963 Heat transfer in annular passages—hydrodynamically developed turbulent flow with arbitrarily prescribed heat flux. *Int. J. Heat Mass Transfer* **6,** 537–557.

KELESSIDIS, V. C. 1986 Vertical upward gas–liquid flow in concentric and eccentric annuli. Ph.D. Dissertation, Univ. of Houston, Tex.

KNUDSEN, J. G. & KATZ, D. L. 1979 *Fluid Dynamics and Heat Transfer.* Krieger, New York.

MYERS, G. E., SCHAUER, J. J. & EUSTIS, R. H. 1963 The plain turbulent wall jet. I. Jet development and friction factor. Technical Report 1, Dept Mech. Engng, Stanford Univ., Calif.

RADOVCICH, N. A. & MOISIS, R. 1962 The transition from two phase bubble flow to slug flow. MIT Report 7-7673-22.

RAJARATNAM, N. 1976 Turbulent jets. In *Development in Water Science,* Vol. 5. Elsevier, Amsterdam.

SADATOMI, M., SATO, Y. & SARUWATARI, S. 1982 Two phase flow in vertical non-circular channels. *Int. J. Multiphase Flow* **6,** 641–655.

SCHWARZ, W. H. & COSART, W. P. 1961 The two-dimensional turbulent wall jet. *J. Fluid Mech.* **10,** 481–495.

SOLOMON, J. V. 1962 Construction of a two phase flow regime transition detector. M.Sc. Thesis, MIT, Cambridge, Mass.

TAITEL, Y., BARNEA, D. & DUKLER, A. E. 1980 Modeling flow pattern transitions for steady upward gas–liquid flow in vertical tubes. *AIChE Jl* **26,** 345–354.

VENKATESWARARAO, P., SEMIAT, R. & DUKLER, A. E. 1982 Flow pattern transitions for gas–liquid flows in vertical rod bundle. *Int. J. Multiphase Flow* **8,** 509–524.

VERHOFF, A. 1963 The two dimensional turbulent wall jet with and without an external stream. Report 626, Princeton Univ., N.J.

WALLIS, G. B. 1969 *One-dimensional Two-phase Flow.* McGraw-Hill, New York.

ZUBER, N. & HENCH, J. 1962 Steady state and transient void fraction of bubbling systems and their operating limit. Part 1. Steady state operation. General Electric Report 62GL100.